Supporting information for

Exploring the Potential of Heteroatom-Doped Graphene Nanoribbons as a Catalyst for Oxygen Reduction

Eduardo S. F. Cardoso[a], Guilherme V. Fortunato[b], Clauber D. Rodrigues[c], Marcos R. V. Lanza[b],

Gilberto Maia[a]*

[a]Institute of Chemistry, Federal University of Mato Grosso do Sul, Av. Senador Filinto

Muller 1555, Campo Grande, MS 79074-460, Brazil

[b]São Carlos Institute of Chemistry, University of São Paulo, Avenida Trabalhador São-

Carlense 400, São Carlos, SP 13566-590, Brazil

[c]State University of Mato Grosso do Sul; Rua Rogério Luis Rodrigues s/n, Glória de
Dourados, MS 79730-000, Brazil

S2

*Corresponding author. Tel: +55 67 3345 3596. E-mail: gilberto.maia@ufms.br (Gilberto Maia)

Table S1. FT-IR attributions for the different doped and undoped GNR samples.

Catalyst	OH stretching vibration from water (cm⁻¹)	Ring stretching (cm⁻¹)	In-plane C-H bending strongly mixed with C—C vibrations or C-N stretching (cm⁻¹)	Ring bending vibration or C-P stretching or C—S stretching (cm⁻¹)	Out-of-plane ring bending (cm⁻¹)	C-S stretching
			Attribution [1,2]			
GNR	3,182 (discreet broad peak)	1,587 (weak peak)	1,150 (weak peak)	1,026 (broad strong peak)	-	
GNRN	-	1,626 (weak peak)	1,203 (broad peak)	1,005 (strong peak)	500 (strong peak)	
GNRS	3,254 (broad strong peak)	Strong peaks at 1,693-1,637 (exhibited two peaks) and 1,527	1,086 (broad small peak)		-	669 (weak peak)
GNRP	3,256 (broad strong peak)	Well-defined peaks at 1,693-1,637 (exhibited two peaks) and 1,530	1,038 (broad strong peak)		-	-
GNRNS	3,240 (weak peak)	Well-defined peaks at 1,693-1,637 (exhibited two peaks) and 1,522	1,095 (broad weak peak)		-	667 (weak peak)
GNRNP	3,252 (broad strong peak)	Well-defined peaks at 1,693-1,649 (exhibited two peaks) and 1,528	1,088 (broad strong peak)		-	-
GNRSP	-	Well-defined peaks at 1,693-1,637 (exhibited two peaks) and 1,526	1,068 (broad weak peak)		-	669 (weak peak)

GNRNSP	3,254 (broad strong peak)	Well-defined peaks at 1,693-1,637 (exhibited two peaks) and 1,522	1,088 (broad strong peak)	-	667 (weak peak)

Table S2. Raman bands attributions for the different doped and undoped GNR catalysts and the I_D/I_G ratio.

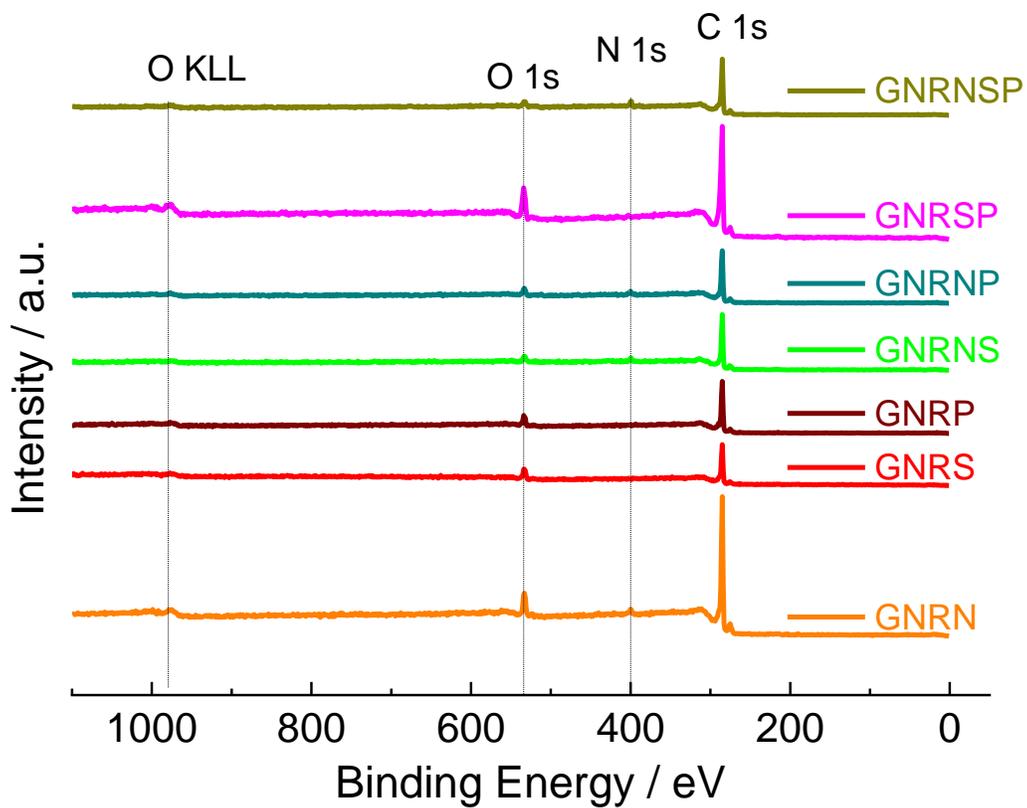| Catalyst	Band (cm⁻¹)						I_D/I_G
	D	G	D+D''	2D	D+D'	2D'	
GNR	1328	1598	2460	2644	2904	3197	1.723
GNRN	1324	1587	2474	2646	2904	3210	1.508
GNRS	1330	1599	2470	2654	2922	3207	2.001
GNRP	1328	1599	2487	2649	2916	3208	1.697
GNRNS	1327	1589	2464	2645	2905	3221	1.789
GNRNP	1331	1605	2463	2656	2919	3234	1.724
GNRSP	1329	1600	2483	2659	2923	3218	1.575
GNRNSP	1328	1600	2442	2655	2920	3219	1.757

Figure S1. XPS survey spectra of the doped GNR samples.

Table S3. Positions, relative sensitivity factors (R.S.F.), atomic and mass percentages obtained from the survey XPS spectra shown in Figure S2 for the doped GNR samples investigated.

Catalyst	Name	Position (eV)	R.S.F.	Content (at. %)	Content (mass %)
GNRN	C 1s	285.00	1.0	89.5	86.9
	N 1s	400.00	1.8	2.5	2.8
	O 1s	533.00	2.93	8.0	10.3
GNRS	C 1s	285.0	1.0	87.8	84.4
	O 1s	533.0	2.93	12.2	15.6
GNRP	C 1s	285.0	1.0	91.0	88.4
	O 1s	534.0	2.93	9.0	11.6
GNRNS	C 1s	285.0	1.0	91.0	89.0
	N 1s	400.0	1.8	3.6	4.0
	O 1s	533.0	2.93	5.4	7.0
GNRNP	C 1s	285.0	1.0	89.7	87.3
	N 1s	400.0	1.8	4.3	4.9
	O 1s	533.0	2.93	6.0	7.8
GNRSP	C 1s	285.00	1.0	89.7	86.7
	O 1s	534.00	2.93	10.3	13.3
GNRNSP	C 1s	285.0	1.0	91.2	89.3
	N 1s	399.0	1.8	4.6	5.3
	O 1s	533.0	2.93	4.2	5.4

Table S4. Elemental analyses of the undoped and doped GNR samples.

| Catalyst	N (wt.%)	C (wt.%)	H (wt.%)	S (wt.%)	O (wt.%)	Others(wt.%)
GNR	1.0	85.2	0.9	0.0	9.7	3.2
GNRN	3.2	85.7	1.0	0.3	4.0	5.8
GNRS	0.2	84.9	1.9	0.0	8.4	4.6
GNRP	0.5	84.3	1.4	0.1	8.8	4.9
GNRNS	5.9	85.8	1.6	0.0	5.0	1.7
GNRNP	3.0	85.2	1.1	0.0	4.9	5.8
GNRSP	0.0	85.2	1.8	0.0	9.8	3.2
GNRNSP	6.2	84.0	2.5	0.0	4.8	2.5
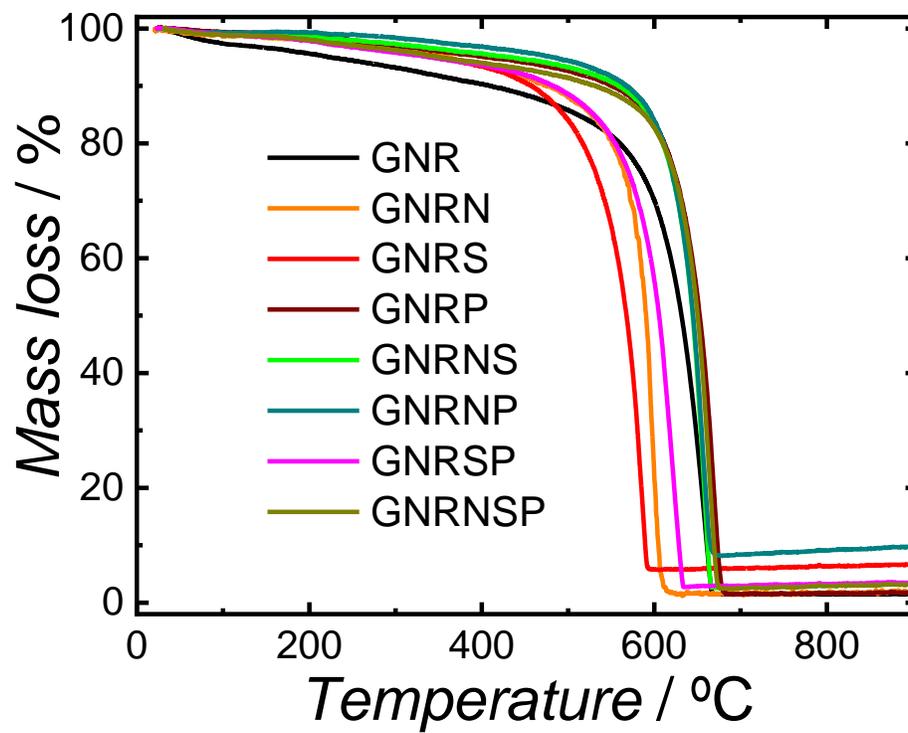
Figure S2. TG curves for the undoped and doped GNR samples.

Table S5. Positions and percentages of the content of functional groups or chemical states present in doped GNR samples obtained from high–resolution XPS spectra shown in Figure 3.

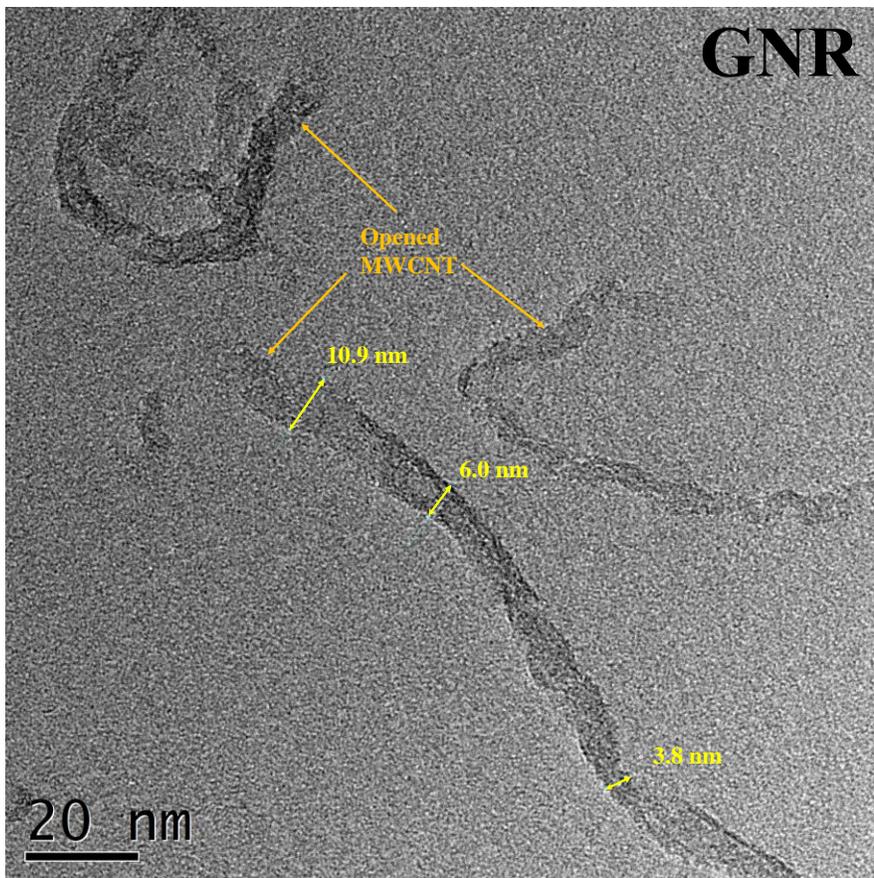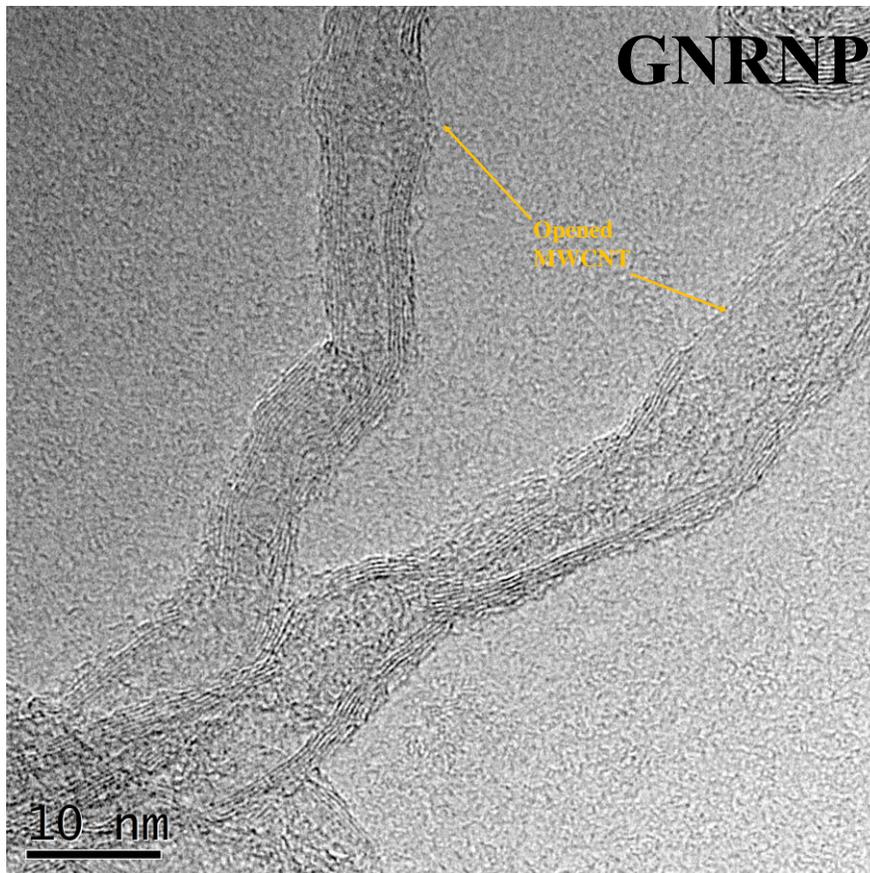| Catalyst	Name	Chemical state	Position (eV)	% content
GNRN	O 1s	C=O	532.3	48.0
		C–O	533.9	52.0
	C 1s	C=C & C-C	284.9	49.3
		C–OH & C–O–C	285.9	38.9
		C–N	287.6	7.3
		C=O & COOH	289.2	3.2
		π–π	290.3	1.3
	N 1s	Pyridinic-N	399.1	18.2
		Pyrrolic-N	400.1	44.2
		Graphitic-N	401.3	32.4
		Oxidized-N	403.7	5.2
GNRS	O 1s	C=O	532.4	48.8
		C–O	534.1	43.2
		H_2O	536.4	8.0
	C 1s	C=C & C-C	284.9	59.2
		C–OH & C–O–C	285.9	19.5
		C–S	286.9	11.8
		C=O & COOH	288.0	3.2
		π–π	289.5	6.3
GNRP	O 1s	C=O	532.5	46.2
		C–O	533.9	49.9
		H_2O	536.8	3.9
	C 1s	C=C & C-C	285	63.6
		C–OH & C–O–C	286	15.6
		C–P	286.7	11.0
		C=O & COOH	287.9	5.4
		π–π	289.5	4.4
GNRNS	O 1s	C=O	532.1	41.9
		C–O	533.8	58.1
	C 1s	C=C & C-C	285	66.2
		C–OH & C–O–C	286	12.6
		C–S	286.7	9.5
		C–N	287.5	5.7
		C=O & COOH	288.6	2.6
		π–π	289.8	3.4
	N 1s	Pyridinic-N	398.5	17.8
		Pyrrolic-N	399.5	28
		Graphitic-N	400.6	48.6
		Oxidized-N	402.8	5.6
GNRNP	O 1s	C=O	532.4	44.9

		C–O	534	55.1
	C 1s	C=C & C-C	285.1	64.8
		C–OH & C–O–C	286	13.7
		C–P	286.7	7.9
		C–N	287.5	6.6
		C=O & COOH	288.7	3.1
		$\pi-\pi$	289.9	3.9
	N 1s	Pyridinic-N	398.9	23.1
		Pyrrolic-N	399.9	35.5
		Graphitic-N	401.2	37.5
		Oxidized-N	403.1	3.9
GNRSP	O 1s	C=O	532.7	43.1
		C–O	534.5	49.3
		H_2O	536.9	7.6
	C 1s	C=C & C-C	285	48.8
		C–OH & C–O–C	286.2	18.1
		C–S	287.0	10.8
		C–P	287.8	8.6
		C=O & COOH	288.8	8.8
		$\pi-\pi$	290.5	4.9
GNRNSP	O 1s	C=O	531.8	51.9
		C–O	533.8	43.4
		H_2O	536.1	4.7
	C 1s	C=C & C-C	285	48.8
		C–OH & C–O–C	286	18.1
		C–S	286.6	6.3
		C–P	287.3	7.3
		C–N	288.3	4.4
		C=O & COOH	289.4	2.2
		$\pi-\pi$	290.6	2.4
	N 1s	Pyridinic-N	398.7	24.2
		Pyrrolic-N	399.6	33
		Graphitic-N	400.8	37.3
		Oxidized-N	402.5	5.5
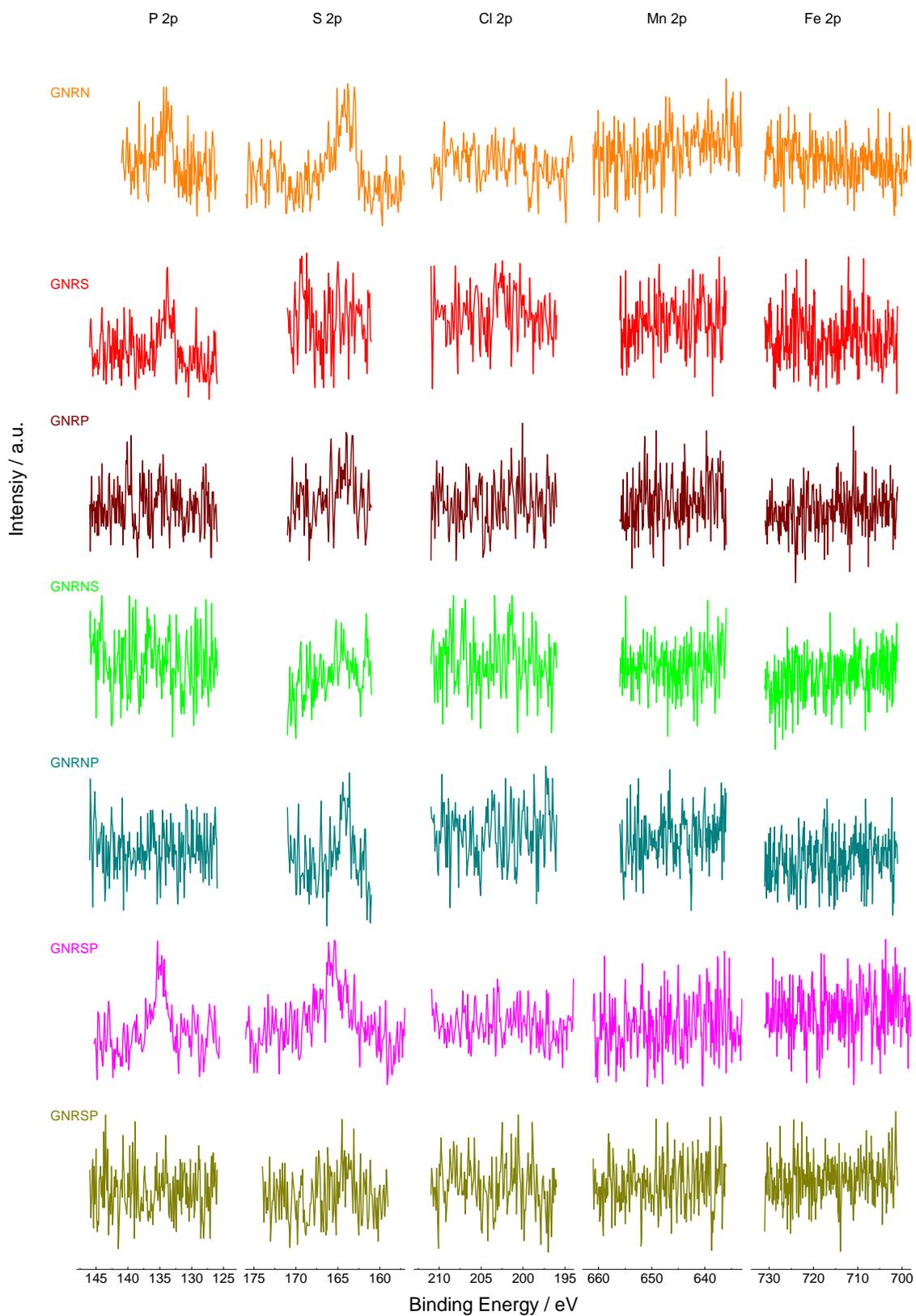
Figure S3. HR-XPS curves for the undoped and doped GNR samples.
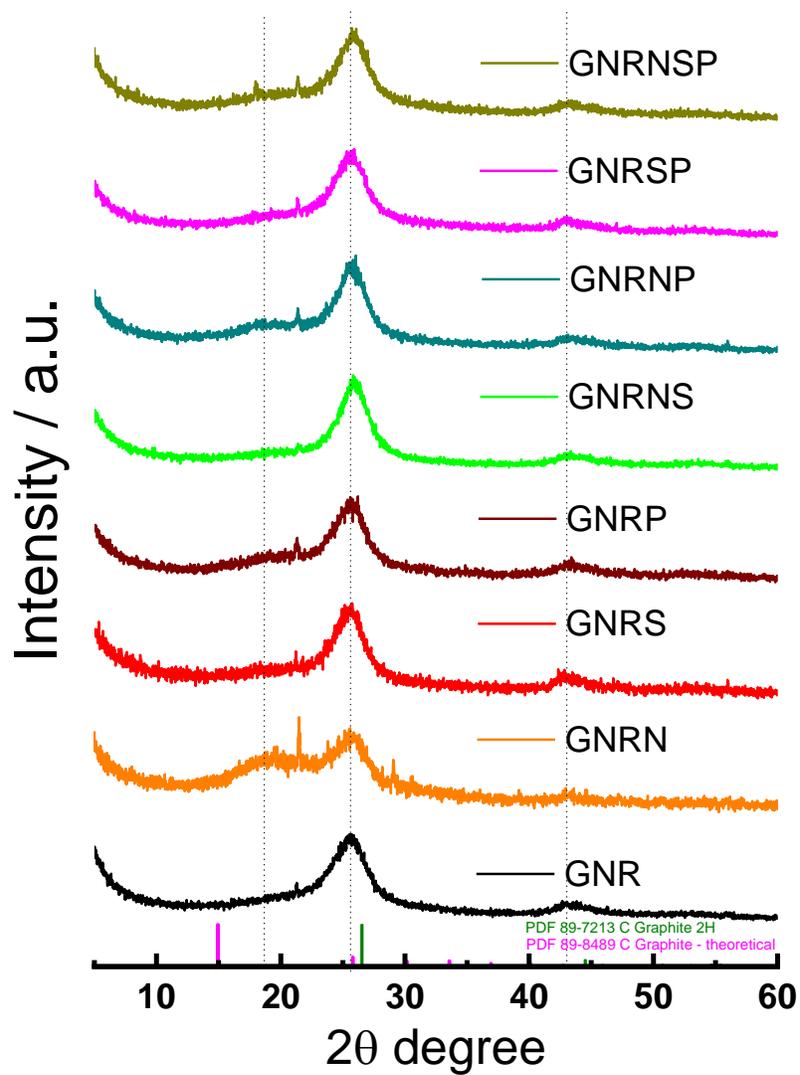
Figure S4. XRD spectra for the undoped and doped GNR samples.

GNR

Opened
MWCNT

10.9 nm

6.0 nm

3.8 nm

20 nm

GNRN

Opened
MWCNT

10 nm

GNRP

Opened
MWCNT

10 nm

GNRNP

Opened
MWCNT
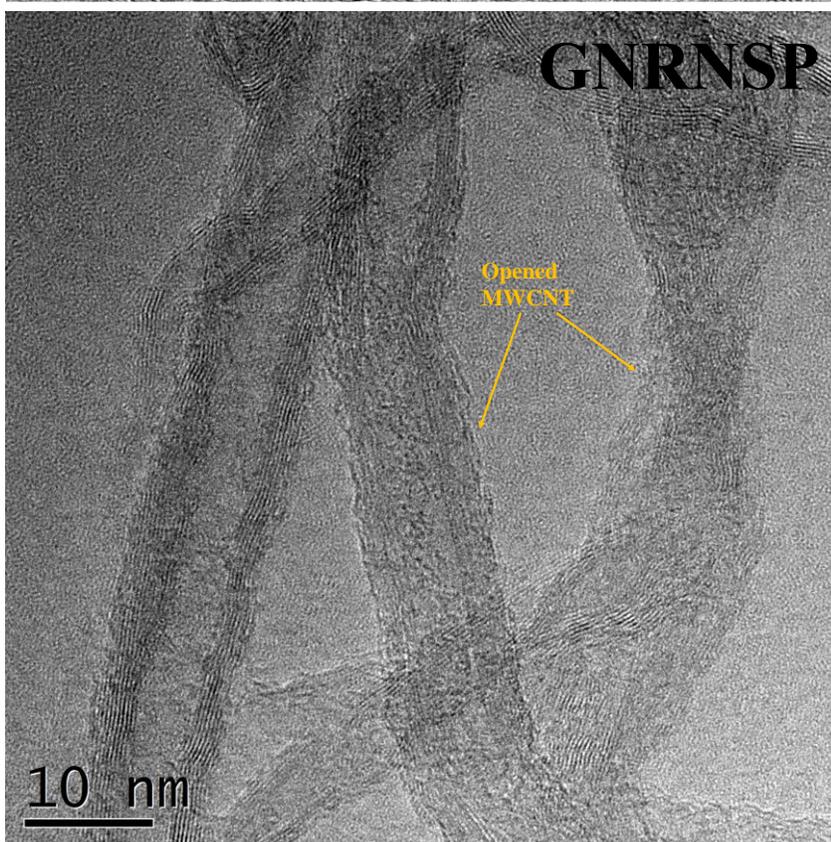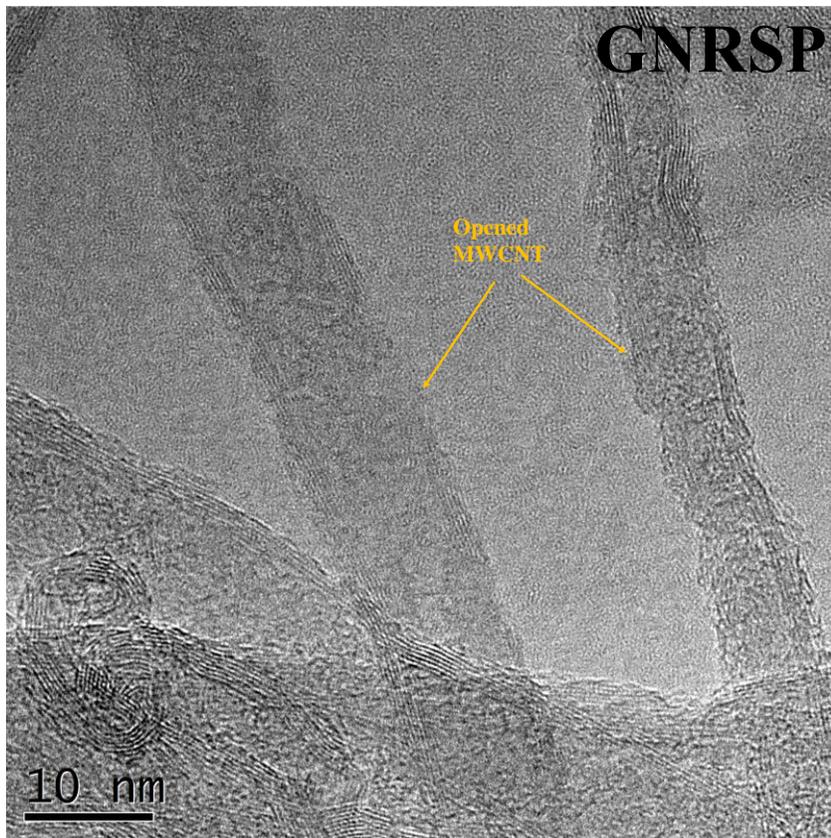
10 nm

GNRSP

Opened MWCNT

10 nm

GNRNSP

Opened MWCNT

10 nm
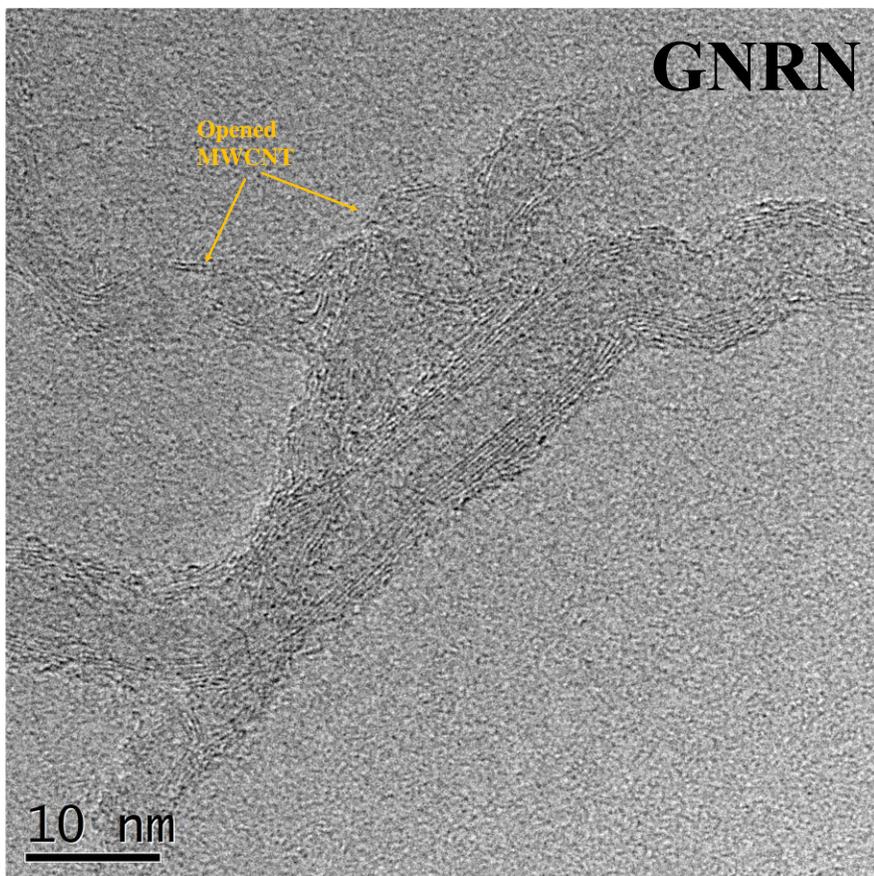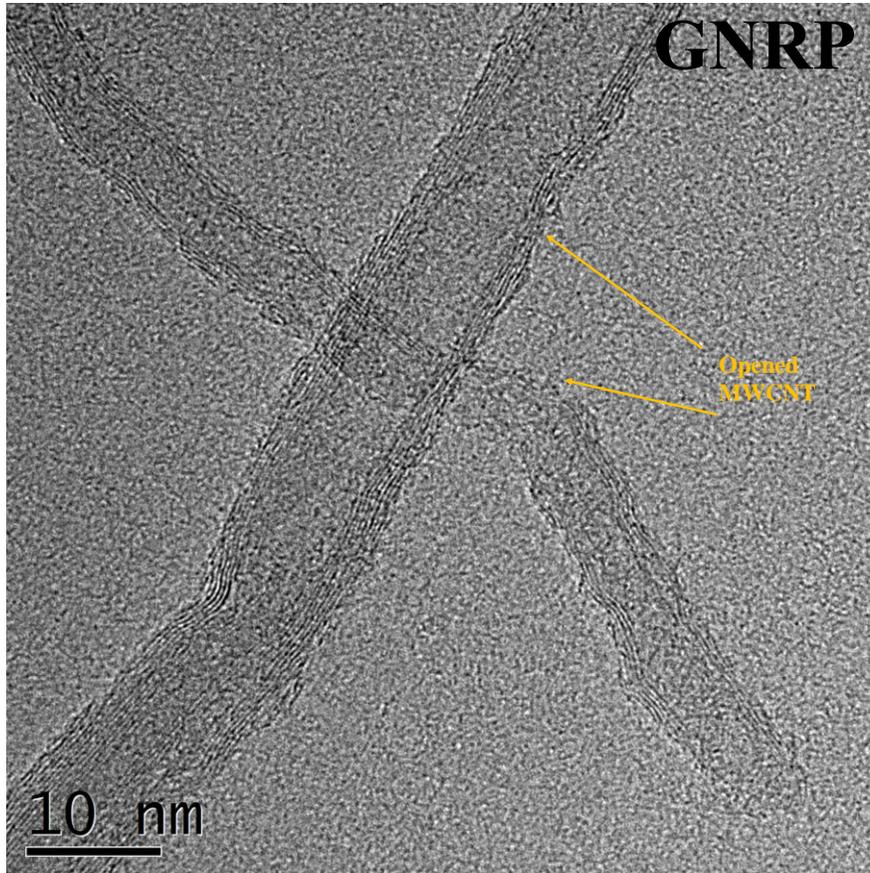
Figure S5. Representative TEM images for the undoped and doped GNR samples.

Table S6. Resistance of electrolytic solution (R_S) values obtained for the glassy carbon (GC) electrode modified with thin-film of undoped or doped GNR samples. The R_S values were obtained from the application of different N_2-saturated electrolyte solutions without electrode rotation using electrochemical impedance (data shown in Figure S5).

Catalyst film	R_S (Ω)		
	in 0.5 M H₂SO₄	*in 0.1 M K₂SO₄*	*in 0.1 M KOH*
GNR	4.68	71.92	36.55
GNRN	4.54	29.71	35.04
GNRS	4.44	30.58	38.82
GNRP	5.91	26.64	38.04
GNRNS	5.24	27.24	35.60
GNRNP	7.76	25.74	46.37
GNRSP	4.89	48.50	36.59
GNRNSP	4.46	33.69	41.00

Figure S6. EIS results for the GC electrode modified with 150 μg cm^{-2} of undoped or doped GNR catalyst. The plane impedance plot was obtained in N$_2$–saturated (A) 0.5 M H$_2$SO$_4$, (B) 0.1 M K$_2$SO$_4$, and (C) 0.1 M KOH using the OCP value as a constant potential for the EIS measurement.
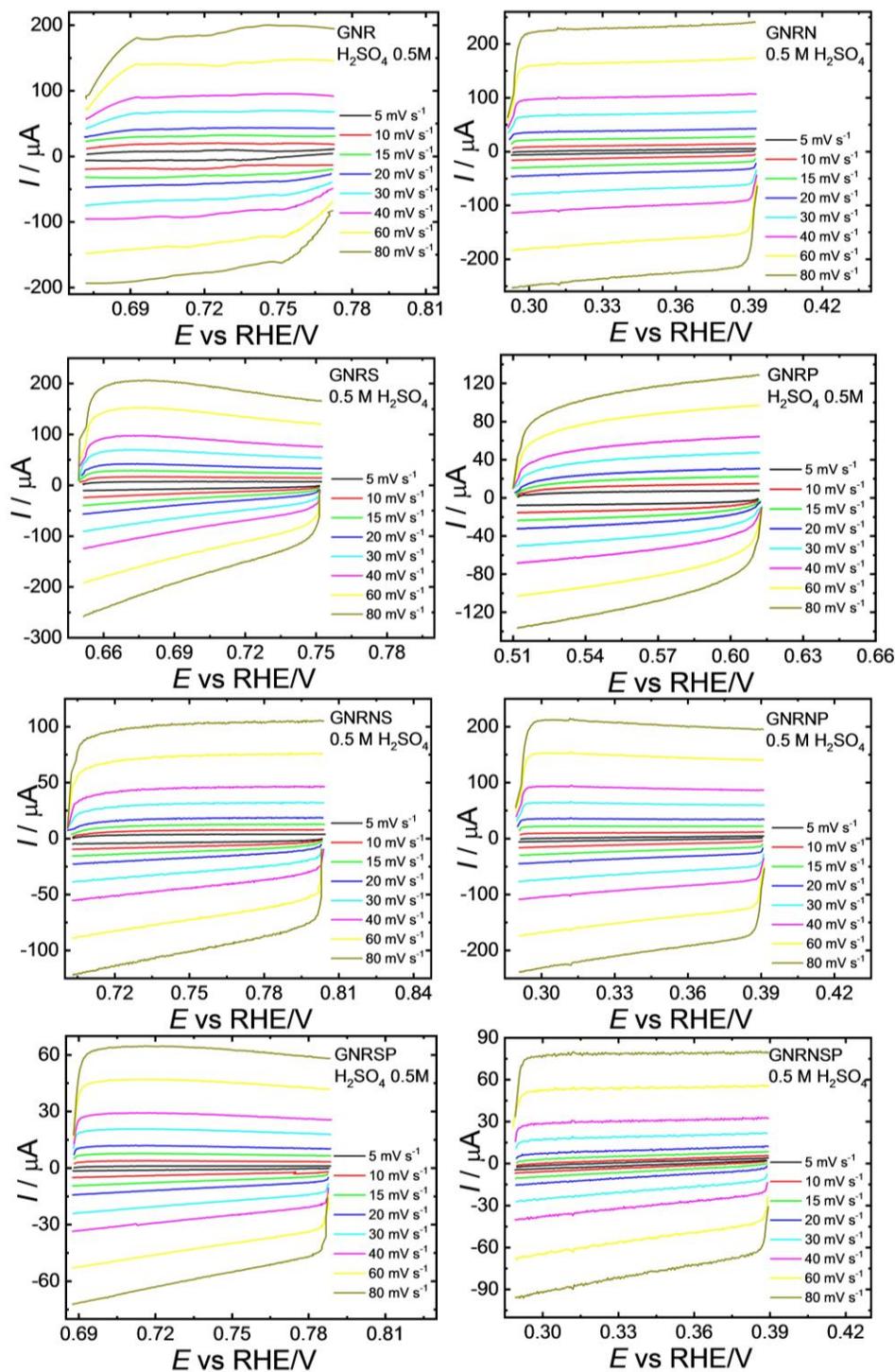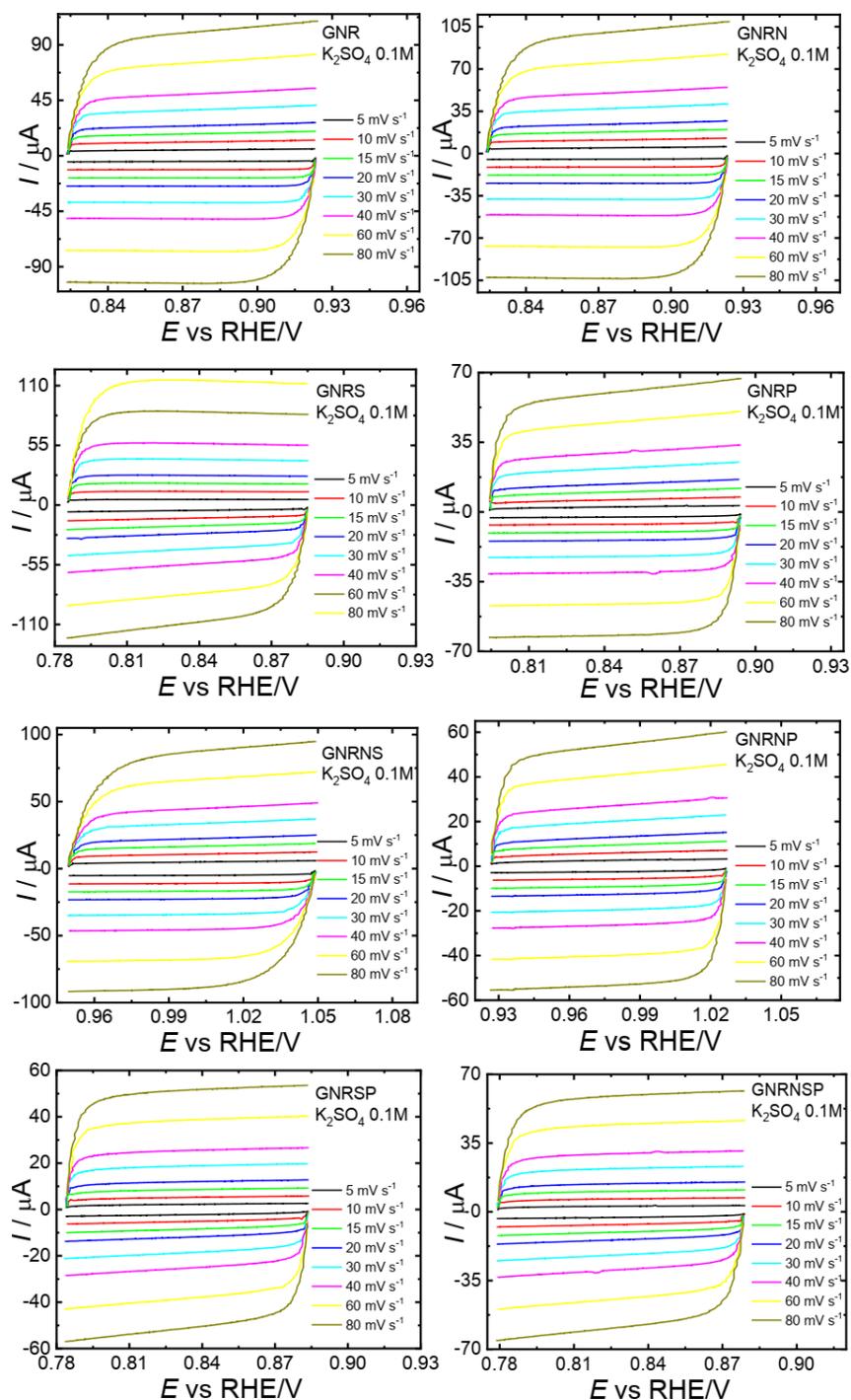
Figure S7. Cyclic voltammograms obtained in a non–Faradaic potential range for the GC electrode modified with 150 µg cm⁻² of undoped or doped GNR catalyst in N₂–saturated 0.5 M H₂SO₄. Prior to the beginning of the subsequent potential sweep, the modified

electrode was kept at each vertex potential for 10 seconds. Scanning was initiated at higher potentials.
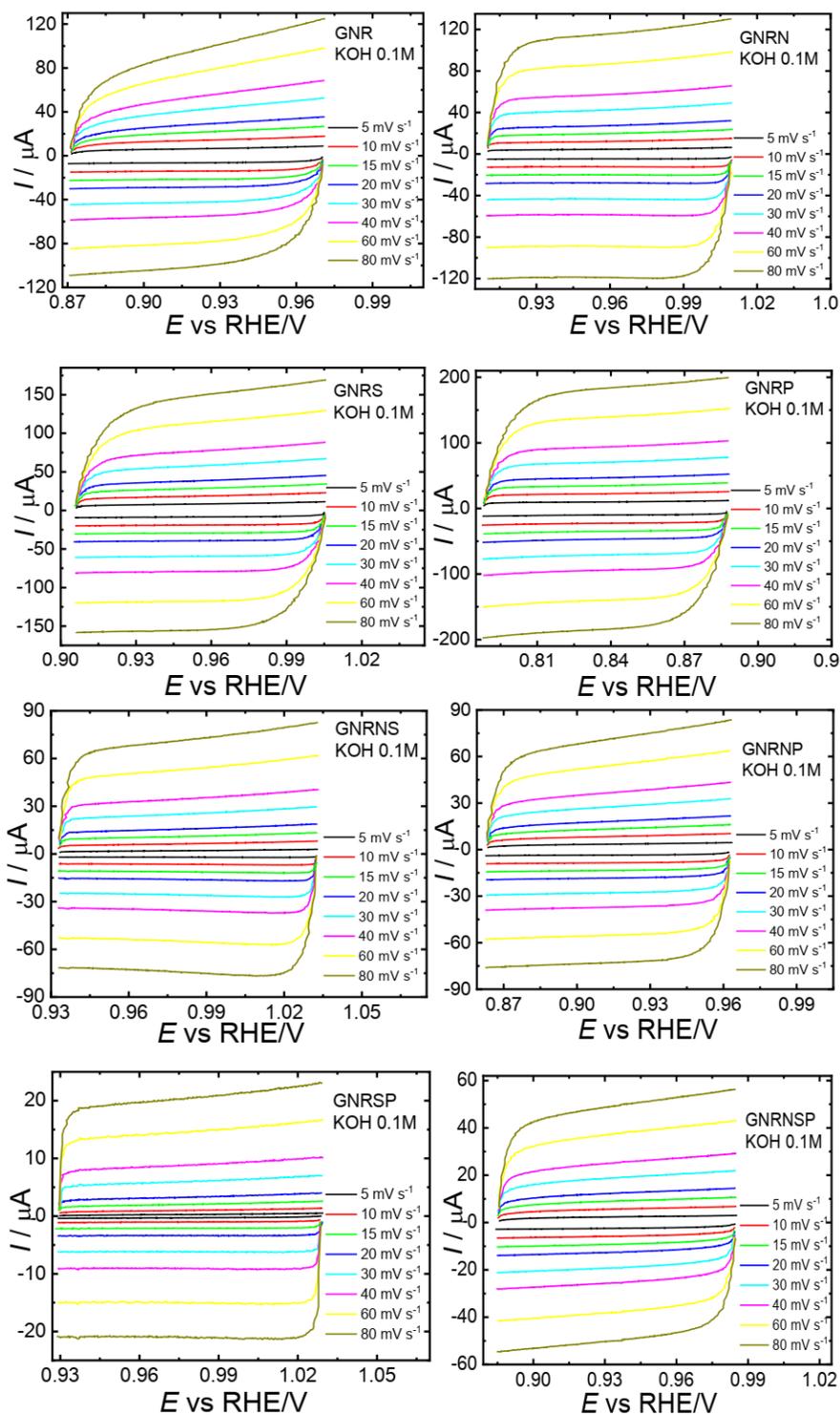
Figure S8. Cyclic voltammograms obtained in a non–Faradaic potential range for the GC electrode modified with 150 μg cm⁻² of undoped or doped GNR catalyst in N₂–saturated 0.1 M K₂SO₄. Prior to the beginning of the subsequent potential sweep, the modified electrode was kept at each vertex potential for 10 seconds. Scanning was initiated at higher potentials.
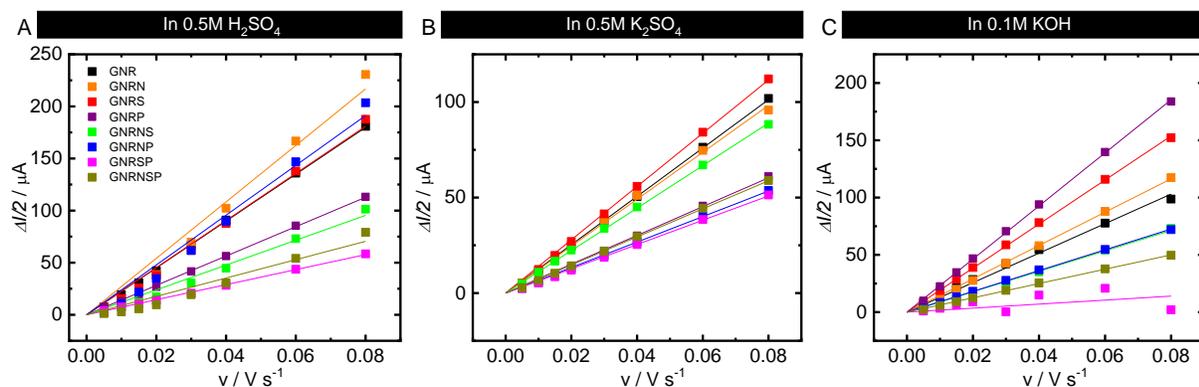
Figure S9. Cyclic voltammograms obtained in a non–Faradaic potential range for the GC electrode modified with 150 μg cm⁻² of undoped or doped GNR catalyst in N₂–saturated 0.1 M KOH. Prior to the beginning of the subsequent potential sweep, the modified

electrode was kept at each vertex potential for 10 seconds. Scanning was initiated at higher potentials.

Figure S10. $\Delta I/2$ *vs.* potential scan rates (v) plots. The plots were constructed based on the differences between anodic (I_a) and cathodic (I_c) double layer charging currents (ΔI) from (A) Figure S7 (obtained in N_2–saturated 0.5 M H_2SO_4), (B) Figure S8 (obtained in N_2–saturated 0.1 M K_2SO_4), and (C) Figure S9 (obtained in N_2–saturated 0.1 M KOH).

The selectivity toward HO_2^- production ($X\,HO_2^-(\%)$) and the average number of electrons transferred per O_2 molecule (n_{av}) were calculated using the data obtained from the RRDE-based analysis (Figure 7) according with the equations S1-2 [3]:

$$S_{HO_2^-} = \frac{2I_r/N}{I_d+\frac{I_r}{N}} \times 100\% \tag{S1}$$

where I_d is the measured disk current, I_r is the ring current, which is given by the HO_2^- oxidation, and N is the efficiency of collection for the ring electrode (N = 0.26).

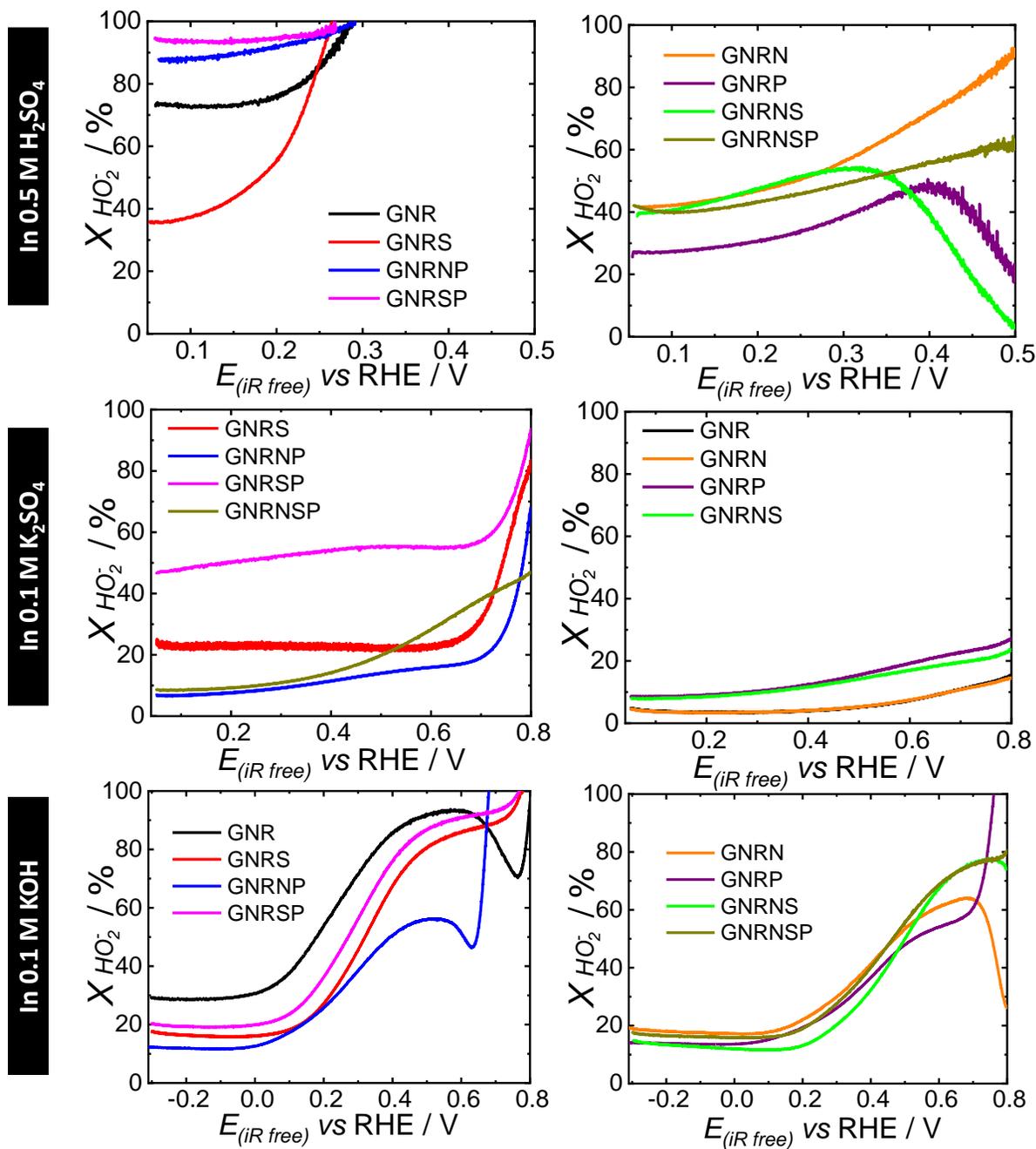$$n_{av} = \frac{4I_d}{I_d+\frac{I_r}{N}} \tag{S2}$$

Figure S11. Selectivity for hydrogen peroxide production ($X_{H_2O_2}$) based on the electrochemical results obtained from LSV analyses conducted in a RRDE system for GC modified with 150 µg cm^{-2} of undoped or doped GNR catalyst (Figure 7) in O$_2$–saturated 0.5 M H$_2$SO$_4$, 0.1 M K$_2$SO$_4$, and 0.1 M KOH (1600 rpm).
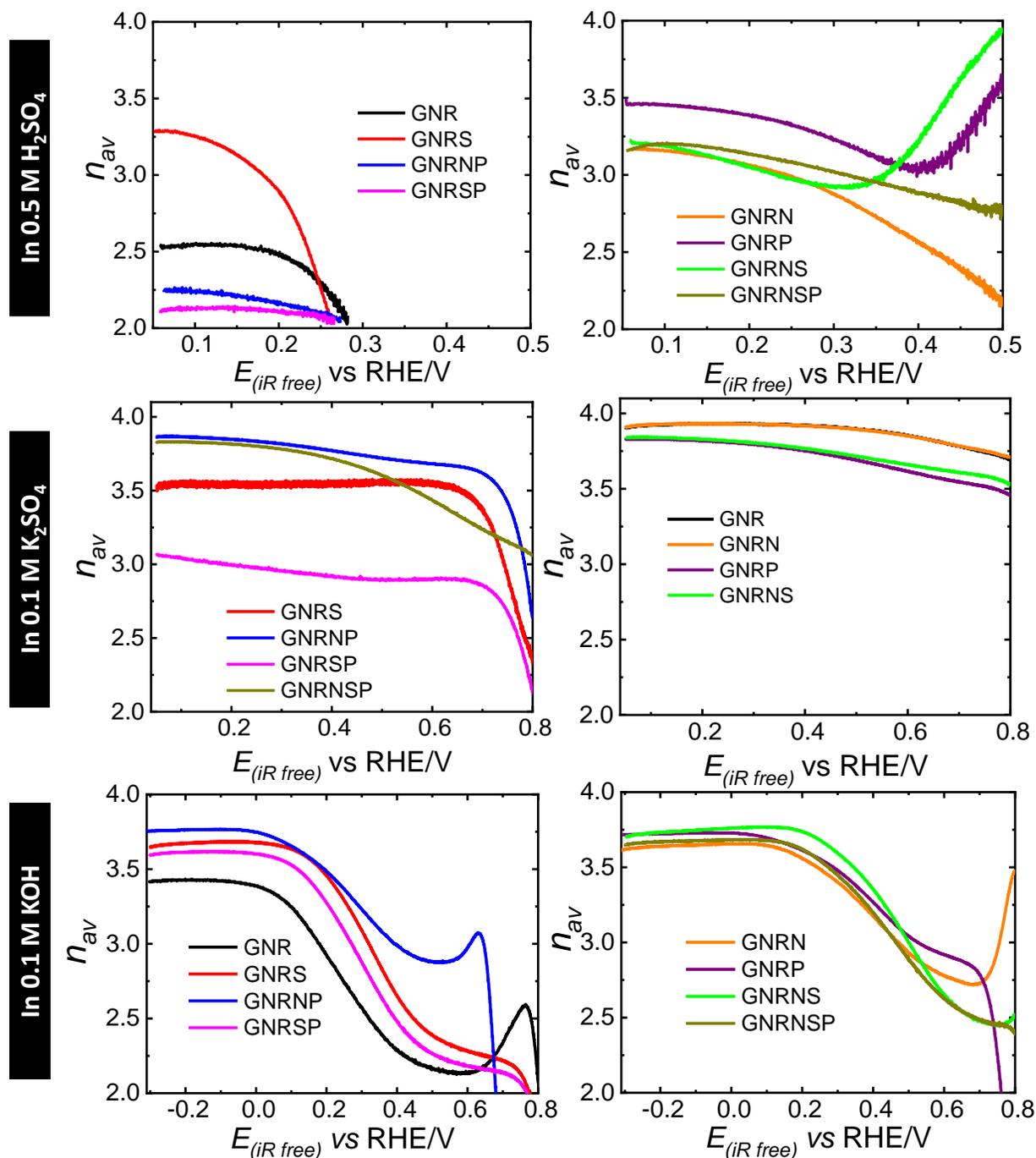
Figure S12. Average number of electrons transferred (n_{av}) during the ORR on the disk electrode at varying potentials based on the electrochemical results obtained from the LSV analyses conducted in a RRDE system for GC modified with 150 μg cm^{-2} of undoped

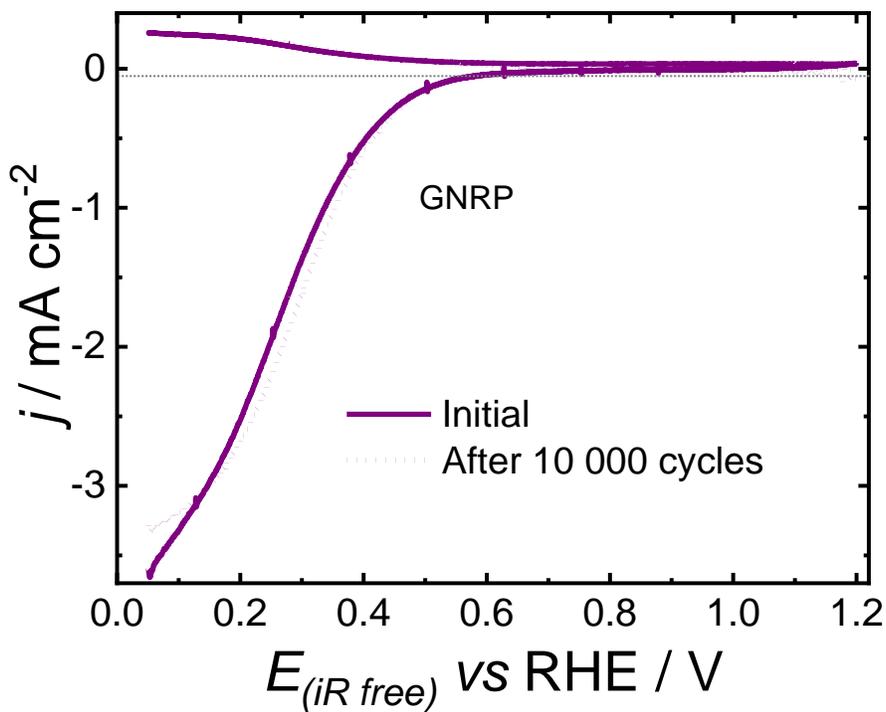or doped GNR catalyst (Figure 7) in O_2^- saturated 0.5 M H_2SO_4, 0.1 M K_2SO_4, and 0.1 M KOH (1600 rpm).

Figure S13. LSV-RRDE curves obtained in O_2^- saturated 0.5 M H_2SO_4 (ω = 1600 rpm, ν = 10 mV s^{-1}, scans were initiated at 0.05 V) for GC electrode modified with 150 μg cm^{-2} of GNRP before and after the application of 10 000 potential cycles.
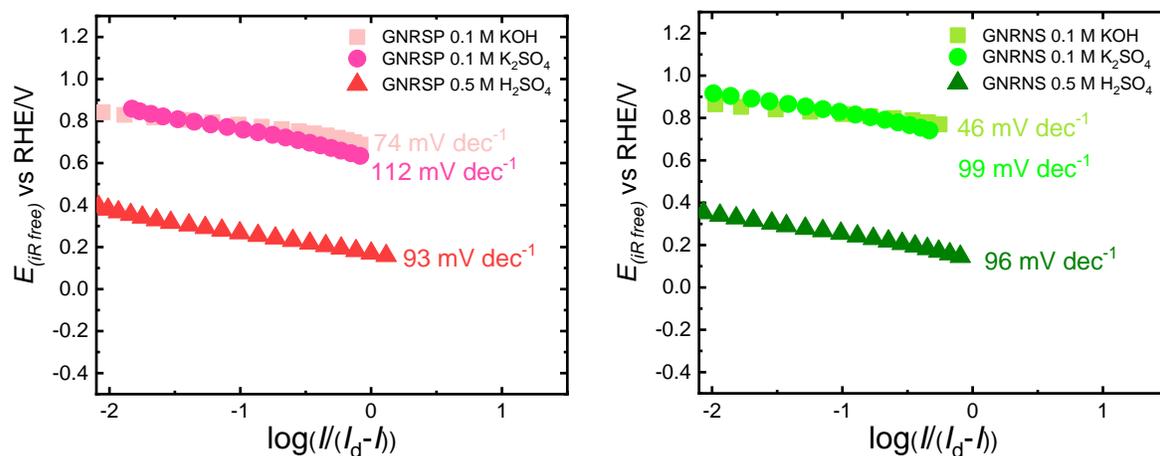
Figure S14. Tafel plots for ORR on (a) GNRSP and (b) GNRNS catalysts obtained in O_2^- saturated 0.5 M H_2SO_4, 0.1 M K_2SO_4, and 0.1 M KOH electrolytes (data extracted from Figure 7).

References

[1]   S.E. Colthup, N. B.; Daly, L. H.; Wiberley, Introduction to infrared and Raman spectroscopy, 3rd edn, Academic Press, Inc., 1990.

[2]   R.M. SILVERSTEIN, F.X. WEBSTER, D.J. KIEMLE, Spectrometric Identification of Organic Compounds, 7th edn, John Wiley & Sons. Inc., 2005.

[3]   G. V. Fortunato, L.S. Bezerra, E.S.F. Cardoso, M.S. Kronka, A.J. Santos, A.S. Greco, J.L.R. Júnior, M.R. V. Lanza, G. Maia, Using Palladium and Gold Palladium Nanoparticles Decorated with Molybdenum Oxide for Versatile Hydrogen Peroxide Electroproduction on Graphene Nanoribbons, ACS Appl. Mater. Interfaces. 14 (2022) 6777–6793. https://doi.org/10.1021/acsami.1c22362.